Lab on a Chip

PAPER

View Article Online
View Journal | View Issue

Cite this: *Lab Chip*, 2025, **25**, 5551

On-chip oocyte cumulus removal using vibration-induced flow

Amirhossein Favakeh, †[a] Amir Mokhtare,†[ab] Hanxue Zhang,[c] Yi Athena Ren[c] and Alireza Abbaspourrad *[a]

Cumulus removal (CR), the removal of the small protective granulosa cells that surround an oocyte, is a crucial step in assisted reproductive technologies (ART). Traditional CR methods rely on vortexing or manual pipetting, which can result in inconsistencies and variability. Here, we present an open-surface platform featuring pillars that actively separates differently sized particles and removes cumulus cells from oocytes through vibration-induced flow (VIF). The platform removed 99% of small particles from the loading chamber by generating a local flow through the pillar array and separating smaller particles from larger particles. The platform was then used to remove cumulus cells from oocytes. CR under different actuation powers, time exposures, and hyaluronidase (HA) concentrations was optimized. The CR of up to 23 oocytes was accomplished simultaneously without any oocyte loss. Finally, mouse cumulus-oocyte complexes (COCs) were inseminated and CR was performed using both manual pipetting (control) and VIF. No statistical difference was observed in the fertilization and blastocyst rates, which were 90.7%, and 50.0% using manual pipetting, respectively, and 93.1% and 43.1% using VIF respectively. This platform automates CR process and reduces the technical manual labor involved in ART, paving the way for standardization and consistency within ART protocols.

Received 28th April 2025,
Accepted 26th August 2025

DOI: 10.1039/d5lc00414d

rsc.li/loc

Introduction

Infertility is a global concern, with declining fertility rates in almost all countries since 1950 creating significant medical, psychological, and social challenges.[1] Advances in assisted reproductive technologies (ART), such as *in vitro* fertilization (IVF) and intracytoplasmic sperm injection (ICSI), offer treatment options and bring hope to those facing infertility.[2]

Oocyte cumulus removal (CR) is an important step carried out to assess oocyte fertilization after insemination in IVF, and it is also vital to evaluate the maturity of the oocyte prior to spermatozoon injection during ICSI.[3,4] Further, CR minimizes cumulus cell contamination to ensure reliable DNA sequencing outcomes.[5] The most common CR technique is based on manual pipetting with an appropriately sized capillary. For IVF, the oocytes are inseminated and then manual pipetting is used to remove the cumulus cells; while for ICSI, two steps are required: enzymatic digestion by hyaluronidase (HA) followed by manual pipetting to remove the cumulus cells.[6] Hyaluronidase digestion occurs effectively between 30 to 120 seconds, depending on enzyme concentration and exposure duration; manual pipetting requires precise timing and careful handling to avoid damaging oocytes and achieve thorough CR.[7] If this method is executed incorrectly, it can lead to unwanted outcomes such as loss of oocytes, zona pellucida fluctuation, large perivitelline space, or even a zona-free egg. This process to achieve CR is dependent on human expertise, requires significant hand-eye dexterity, and thorough training. This technique is time-sensitive, labor-intensive, and inefficient. Therefore, many of these challenges could be resolved by controlling and automating CR procedures, ideally while using a minimal amount of enzyme.

To overcome these challenges, microfluidic platforms have been integrated with ART for automating CR.[8,9] Over the past two decades, microfluidics platforms have been developed for oocyte analysis,[10] sperm selection,[11–13] embryo culture,[14] insemination,[15] and cryopreservation.[16] The extraction of single cells from microfluidic channels, however, has presented a persistent challenge.[17] Unfortunately, oocytes are often lost in the interface between the channel and the external environment, such as tube connections, and microfluidic platform designs, to date, have made it difficult to identify and collect the cells for post-analysis.[18]

Open surface chips have been used for various biomedical applications because of their lower cost and ease of use, enabling cell drops or collection sites with a lowered risk of

[a] *Department of Food Science, College of Agriculture and Life Sciences (CALS), Cornell University, Ithaca, New York, 14853 USA. E-mail: alireza@cornell.edu*
[b] *Center for Technology Licensing, Cornell University, Ithaca, New York, 14853, USA*
[c] *Department of Animal Science, College of Agriculture and Life Sciences (CALS), Cornell University, Ithaca, New York, 14853 USA*
† These authors contributed equally to this work.

cell loss. These chips can be mass-produced and are single-use, which reduces potential contamination in clinical and biological laboratories.[19] They also provide opportunities to integrate other technologies for on-chip cell manipulations.[20]

Biomedical applications for active flow mixing and cell manipulation on a chip have emerged where the flow is controlled externally by optical forces,[21] micromanipulators,[22] acoustic waves,[23] electric fields,[24] and magnetic forces.[25] Optical tweezers can manipulate a single cell with high position accuracy;[26] however, this technique is limited to manipulating small cells since it offers weak (~pN) forces with a small trapping area (~100 μm). Operating micromanipulators demands both complicated systems and highly skilled operators. Cell manipulation by surface acoustic wave[27] or dielectrophoresis[28] requires the fabrication of piezo actuators or multi-electrodes on a chip, which adds to the complexity of the fabrication process and control system. Magnetic fields require that a pre-magnetized label be added to the cells, which is not an ideal condition for cells destined for ART.[29] Among all these external forces, only vibration-induced flow (VIF) has been used to directly manipulate cells and microparticles in a simple label-free system.[30,31]

VIF is the science of acoustic streaming generated around the microstructure of a chip using periodic vibration.[32–34] This technique is easy to control and apply to an open-surface chip structure for precise microscale manipulation on an *XY* piezoelectric stage.[30] As a result, several studies have focused on the transportation,[35] rotation,[30] manipulation,[36] and gathering[19] cells by applying VIF to the predefined trajectory of micropillars on the open surface chip. The induced flow around the micropillars using VIF is controlled by changing the applied frequency, amplitude, and shape or arrangement of the micropillars.[32] Thus far, different micropillar arrays have been reported.[35–38] This leads to improved manipulation consistency and enhanced performance on an open surface chip.[39]

Despite the advantages of microfluidics and, specifically, open-surface chips, there have been relatively few studies on female gamete processing on these platforms.[40] Zeringue *et al.*[8,9] created a microfluidic channel that can trap the cumulus–oocyte complexes (COCs), facilitating oocyte denudation. Another microfluidic channel was proposed by Weng *et al.*[10] where the cumulus cells were removed from the oocyte when the cells were guided through the sharp, corrugated microfluidic channel walls. We have previously reported the use of a microfluidic channel using a non-contact oscillation technique where the cumulus cells were shaken away from the oocyte.[41] These devices, however, still require additional steps for preparing and loading the cells; cells were often lost in the microfluidic channel, and they still required a skilled technician for the final cell harvest. A robotic system was introduced to accomplish conventional CR; however, it still required a microscope and micromanipulators, making it costly and cumbersome.[42]

We have used acoustic waves for oocyte manipulation and CR,[43] and in another study, the cumulus cells from a batch of oocytes were removed using acoustic forces inside a microwell within a few minutes.[40] Although the loading and collecting of the cells was easier, and did not require a highly-technical skillset, controlling the temperature variation due to the applied acoustic streaming was challenging.

Building on our previous work, we report on the use of a disposable open-surface chip that uses vibration for CR in a thermally stable environment. We developed an *XY* piezoelectric stage that applies a circular VIF *via* periodic vibrations to the chip mounted on the stage at the microscale to move the cells or particles through pillars. This chip has high-throughput for cell or particle separations, transportation, and can be used for oocyte cumulus denudation.

We first studied the effect of applied actuation power and time exposure on the velocity to examine microparticle removal from a loading chamber *via* this system. Our chip design allowed for nearly all small particles to be cleaned (removed from the loading chamber), resulting in a 99% cleaning efficiency of the loading chamber within less than 20 seconds, followed by particle separation (80 μm from 13 μm).

This chip was then used to remove cumulus cells from oocytes. The smaller cumulus cells were directed from the loading chamber to an annulus well surrounding the pillar assembly while the cleaned oocytes remained in the loading chamber. This chip allows users to load and collect the cells easily and to remove the cumulus cells noninvasively from the oocyte in a thermally stable environment. Finally, to evaluate the safety of this system, COCs inseminated using conventional IVF were subjected to CR using VIF *versus* manual pipetting. Both groups were then tracked through all stages of preimplantation development and the outcomes compared.

Concept, design, and operating principle

Numerous studies have explored the interaction between vibrating objects and fluid behavior.[44,45] Using VIF, a local flow can be created with a circular symmetric motion around a micropillar at a microscale (Fig. 1a). We used numerical simulations to help us understand the induced flow around the single circular pillar (Fig. S1 and S2). When micropillars are patterned on a chip, if the distance between the pillars is shorter than the circular rotational movement around each pillar, a global whirling flow (a rotationally symmetric flow pattern) is induced along the array of pillars (Fig. 1b). This whirling flow can then efficiently capture and transport cells or particles, and their efficient movement is dependent upon variables such as flow-induced distance (δ), cell/particle size (d), pitch (p), and micropillar radius (a).

Reported here is a platform with a micropillar array configuration designed to separate and extract single cells (Fig. 1c). We designed the pillar array on an open surface

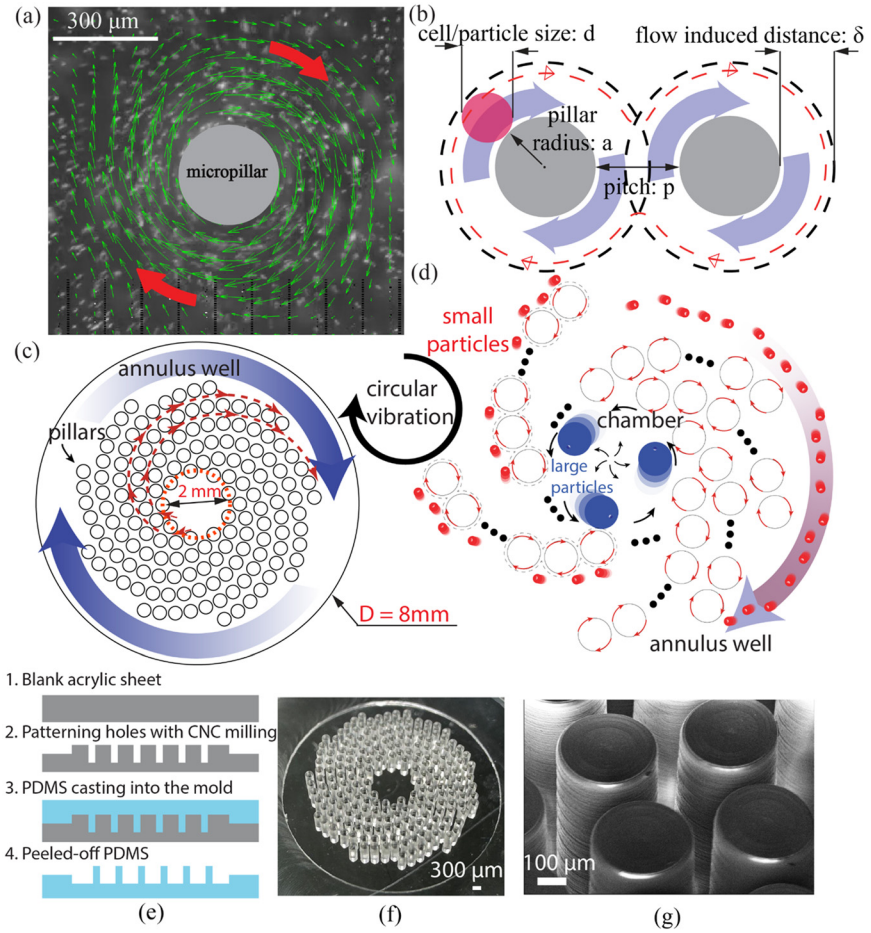

Fig. 1 On-chip cell manipulation, transportation, and separation using vibration-induced flow (VIF). (a) Microscope image of induced circular flow around a single pillar due to applied circular vibration (green arrows show the flow direction). (b) Transportation flow caused by circular vibration through the array of pillars. Red dashed lines indicate induced flow through the pillar array. (c) Topographical feature of induced flow by circular vibration through the spiral pillar array for the proposed chip. *D* is the chip diameter. (d) Particle size separation using VIF. (e) Open surface chip fabrication process. (f) Fabricated chip with the pillar array. Pillar height is 1.1 mm, and annulus well wall height is 300 μm. Pillar diameter is 300 μm. (g) Scanning electron microscope (SEM) image of the fabricated pillars.

chip to keep larger cells/particles inside the loading chamber while guiding smaller cells/particles to the annulus well along the spiral pillar array (Fig. 1d). To achieve this, our designs require the pitch (p) to meet the condition where the diameter (d) of the small cell/particle is less than p, alternatively, the diameter of large cell/particle exceeds that same value, such that $d_{small} \leq p \leq d_{large}$.[46] For example, given that the small and large cell/particle diameters are 13 and 80 μm, respectively, we determined that the pitch values should fall within the range of $13 \leq p \leq 80$ μm. Therefore, we chose the distance between each pillar in an array as 70 μm. This allowed for the smaller particles to move along the spiral pillar array while keeping the larger particles in the loading chamber.

The chip's design included three sections: (1) the loading chamber, (2) the spiral pillar array, and (3) the annulus well. The loading chamber for injecting the cells or particles consists of a closed loop of circular pillars designed around a central diameter of 2 mm. The target large particles or oocyte cells (maximum size 120 μm without considering the cumulus) swirl in the loading chamber, the interior of the circular pillar loop, and cannot pass the pillars because they are larger than the pitch value between the pillars. The loading chamber diameter is designed to allow the operator enough access to drop and collect the cells easily. The spiral pillar arrays are structured around the chamber area, and they lead from the chamber zone to the annulus well. Finally, the annulus well collects the separated small cells or particles and prevents them from reentering the spiral pattern.

Experiment setup and conditions

The *XY* piezoelectric stage[47] was fixed on top of the Unitron Z12 Stereoscope stage (Fig. S3). Two piezoelectric actuators (PEA) were embedded in the *XY* piezoelectric stage along the *X* and *Y* axes to apply rotational VIF to the chip (Fig. S4). A rotational closed-loop movement was applied to the micropillars by transferring the sinusoidal forces in the *X* and *Y* directions with a 90-degree phase offset using the waveform generator Moku Go (Liquid Instruments Model

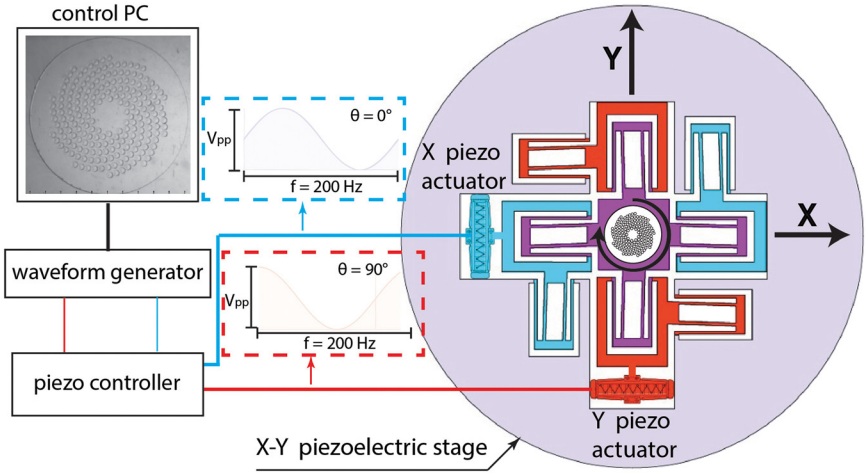

Fig. 2 Graphical representation of the experimental setup. Two piezoelectric actuators (PEA) are embedded in the demodulated stage along the *X* and *Y* axes (additional details can be found in the SI). Sinusoidal forces in the *X* and *Y* directions with a 90-degree phase offset from the waveform generator were amplified through a high-voltage amplifier to apply rotational vibration to the chip fixed on the stage.

M1). The voltage was amplified *via* a 3-Axis Piezo Controller (Thorlabs, Newton, NJ, USA. Product number: MDT693A) high-voltage amplifier (Fig. 2). The direction of the flow can be changed by switching the signal phase applied to the system. Also, the flow velocity can be adjusted by changing the actuation power to a maximum of 1.5 V_{pp} (peak-to-peak). For faster cell/particle transportation and oocyte cumulus denudation, the vibration frequency was set to 200 Hz as it applies the strongest steaming effect.[19] The chip was placed on a PDMS slab with a thickness of 3 mm to establish a connection between the chip and the *XY* piezoelectric stage. Therefore, the applied vibration propagates through the PDMS slab to the chip with the embedded micropillar array. The microscopic images were recorded *via* a Phantom high-

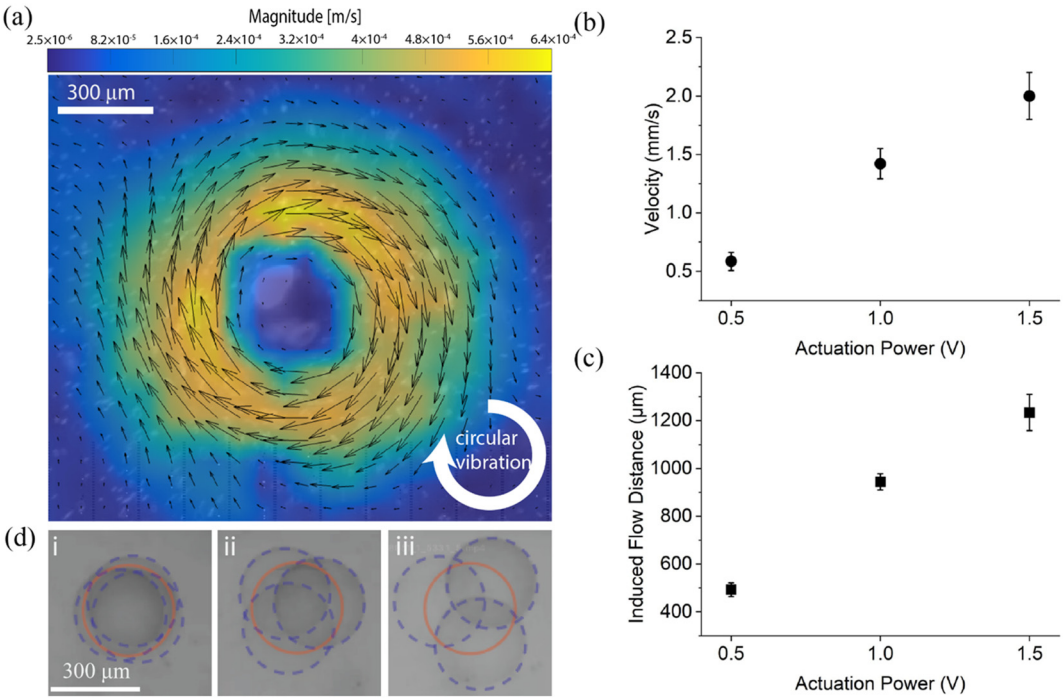

Fig. 3 Induced flow around an open surface single pillar *via* circular vibration induced flow (VIF). (a) Particle image velocimetry (PIV) analysis of the induced flow around a single pillar with a diameter of 300 µm and height of 1100 µm when V = 500 mV_{pp} and f = 200 Hz. Color contour represents the velocity magnitude, and vectors show the flow field direction. (b) Effect of applied actuation power on velocity and (c) pitch distance induced around a pillar. (d) Pillar displacement with respect to the applied actuation power. The red circle pillar represents the stable condition of the pillar before the applied actuation power, while the dashed blue pillars illustrate the displacement of the pillars when subjected to vibration amplitudes of (i) 500 mV_{pp}, (ii) 1 V_{pp}, and (iii) 1.5 V_{pp} within 200 Hz applied frequency.

speed camera controlled by a PC. We set the image acquisition frame rate to 200 fps since the applied frequency is 200 Hz, so instantaneous particle or cell movement was tracked without blurring. The exposure time was set to 4900 μs. Also, because PDMS is a hydrophobic material, to avoid trapping air bubbles around the pillars in the presence of the media and to make the surface hydrophilic, the chips were exposed to oxygen plasma (Plasma cleaner Harrick Plasma) for 3 min before loading the particles or oocytes. This technique has been widely reported as a safe and non-toxic treatment for biological samples,[48] including oocytes.[10,49]

Results and discussion

Induced flow around a single pillar by circular VIF

The magnitude of velocity around the pillars was assessed by varying the applied VIF amplitudes, raising the actuation power from 500 mV_{pp} to 1.5 V_{pp}. The flow was evaluated around a single pillar on a separate chip featuring one pillar with the same diameter and height as the pillars in the spiral array (Fig. 3a). The water mixture contained fluorescent particles, each with a diameter of 13 μm and a concentration of 7.53×10^8 particles per mL. The height of the solution mixture in contact with the pillar was approximately 300 μm. Our results show that the flow velocity was dynamically controlled by the actuation power (Fig. 3b). Increasing the actuation power increases the velocity around each pillar, subsequently increasing the induced flow distance around the pillar (Fig. 3c). This open chip design provides a larger parameter value for velocity and induced flow distance than previously reported, as we have not used any oil or glass on top of the pillars.[30] The center displacement of the pillar when subjected to vibration amplitudes of 500 mV_{pp}, 1 V_{pp}, and 1.5 V_{pp} within 200 Hz applied frequency is 33 μm, 75 μm, and 110 μm, respectively (Fig. 3d).

Chamber cleaning efficiency

Chamber cleaning efficiency refers to the VIF's ability to actively sweep small, undesirable microparticles or cell debris from the loading chamber during operation. This cleaning effect keeps the area free of residual particles, essential for consistent separation performance and preparing a clean zone for biological applications. After the chip was surface treated, 18 μL of Milli-Q water was dropped directly onto the chip, followed by 2 μL of Milli-Q water containing 13 μm particles at a concentration of 7.53×10^8 particles per mL, dropped into the center of the loading chamber. Then, different actuation powers ranging from 500 mV_{pp} to 1.5 V_{pp} were applied to determine the best power for the highest cleaning efficiency. A clockwise rotational vibration resulted in most of the small particles being removed from the chamber (Movie S1). Particles were mechanically transported and pushed to the annulus well through the spiral pillars by the whirling flow over the pillar array. Some particles did get stuck between the pillars, possibly because they were trapped by the recirculating flows between the spiral pillar array. By increasing the distance between each spiral array, this effect was mitigated. The spiral pillar array directs the particles toward the annulus well. Then, because the flow of the annulus well is in the same direction as the whirling flow through the pillars, particles located in the annulus well slip over the outside pillars in contact with the well, become trapped by the direction of the flow and can no longer enter the spaces between the pillar array (Movie S2). Eqn (1) can be used to calculate the loading chamber cleaning efficiency *via* VIF:

$$E_c = \frac{(N_0 - N_t)}{N_0} \quad (1)$$

where E_C is a function of the applied actuation power and operational exposure time, N_0 is the number of particles that we drop into the loading chamber initially, and N_t represents the number of particles that remain at time t. There is little difference in the amount of E_C after 1 min, so we operated the system for 1 min exposures. Increasing the applied actuation power increases the E_C of the chamber (Fig. 4a). The highest efficiency for loading chamber cleaning was achieved at the highest actuation power amplitude (1.5 V_{pp}). We reach 99% particle cleaning efficiency in under 20 s, leading to an area that is nearly spotless (Fig. 4b and c, Movie S1).

The higher actuation power generated a faster whirling flow along the pillar array, moving the particle along faster due to higher hydrodynamic forces. Increased vibration actuation power boosts the fluid flow around the pillars, creating greater shear forces that surpass the adhesive forces acting between the particles and the chip surfaces. This process facilitates effective particle transport through the spiral pillars and finally repels the particles to the annulus well.

At lower applied actuation power, the fluid flow is too slow to move the particles efficiently in the chamber area. This is because the diameter of the chamber area is larger than the distance between the pillars. Therefore, the weak induced flow around the pillars surrounding the chamber cannot efficiently move the particles, and due to the available vortex in the loading chamber area, the rest of the particles remain in the center of the chamber area. The incidental vibration that results from the collisions between the pillars and the particles can impact the trajectories of the particles.

Particle separation

A mixture of different-sized particles was used to show that smaller particles would be swept from the loading chamber while larger particles would be retained. The experimental procedure follows the earlier process, but instead of a particle of a single size, a combination of 80 μm and 13 μm particles was loaded into the loading chamber. When rotational VIF was applied to the chip, it created enough of a flow to sweep the smaller particles out of the loading area, while larger particles moved in a circular closed loop inside the chamber. Since the diameter of larger particles is larger than the distance between the pillars, the larger particles do not move

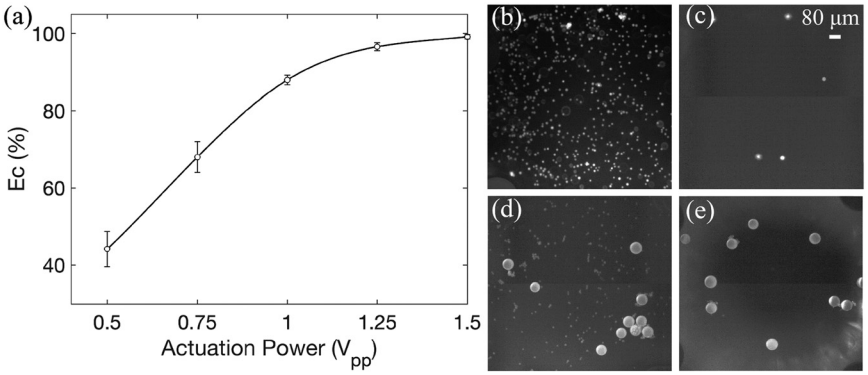

Fig. 4 The influence of vibration-induced flow (VIF) on particle removal efficiency from the loading chamber area. (a) Calculated cleanness based on the actuation power applied for t = 60 s. Error bars indicate the standard deviation from three experiments. Image from the recorded experiment (Movie S1) at (b) t = 0 s before applying the actuation power and (c) t = 23 s after applying the actuation power. Image from the recorded experiment (Movie S3) where two different-sized particles were separated (d) t = 0 s before applying the actuation power and (e) t = 23 s after applying the actuation power.

through the spiral pillar array, and they remain inside the chamber without being lost (Fig. 4d and e, Movie S3). Because the smaller particles were removed from the loading chamber during operation, it is very easy to collect the 80 μm particles from the chamber using pipettes.

Vibrational approach for ova denudation

Mouse oocytes were used as the target cells because they share a substantial degree of genetic homology with humans.[50] Mouse COCs consist of a large oocyte, which is roughly 100 μm in diameter, and is surrounded by smaller cumulus cells that are about 20 μm in diameter in an extracellular matrix spanning 400–700 μm. Using circular VIF with our platform, we denuded the oocyte of cumulus cells. The smaller cumulus cells were transferred to the annulus well, while the clean oocyte remained inside the loading chamber in the CR process (Fig. 5a and b). CR in this system involves three steps: (1) loading, (2) denudation, and (3) extraction of the cleaned oocyte.

The chip was loaded with 18 μL of the M2 media with 15.25 IU mL^{-1} HA. Then, COCs were added to the loading

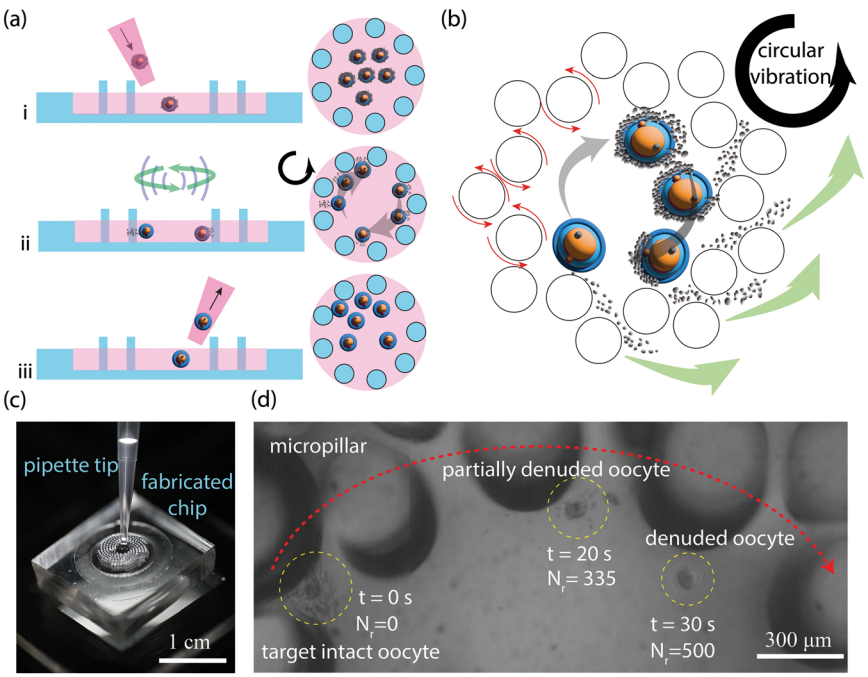

Fig. 5 Vibrational approach for ova denudation. (a) Working mechanism of vibration-induced flow (VIF) on oocyte denudation. (i) Loading. (ii) Denudation. (iii) Extraction. (b) Illustration of circular vibration oocyte denudation. (c) Image of oocyte being loaded into the chamber area using 1 mm pipette tip. (d) Stacked images of freeze/thaw oocyte denudation within the loading chamber at different times (t) and different numbers of rotations (N_r) using 15.25 IU mL^{-1}. Hyaluronidase (HA) and applied actuation power of 1.5 V_{pp}.

chamber using a 1 mm pipette tip (Fig. 5c). Since the distance between the pillars is smaller than the diameter of the COCs and the oocytes, they will remain in the loading chamber. A delay of 60 s before applying vibration was used to allow the HA to loosen the cumulus cell matrix.

The whirling flow caused by VIF allowed the oocytes to circulate in a closed loop of the loading chamber and bump against the pillars. The smaller cumulus cells detach from the oocyte due to the shear force that is exerted by the chamber pillars. Stacked microscopic images show the gradual denudation of the oocyte at different numbers of rotations (N_r) (Fig. 5d). They illustrate both the ability to separate smaller cells from larger ones and the movement of larger cells within the loading chamber using VIF. The smaller cumulus cells leave the loading chamber, are driven through the spiral pillar array, and are collected in the annulus well. The circulating flow that is generated along the pillars in contact with the well washes the cumulus cells away from the loading chamber and keeps them from returning to the spiral array. The vibration continues until we visually confirm that the cell is cumulus-free (Movie S4). We measured the denudation time with a stopwatch.

After oocyte denudation, the system is turned off. The cumulus-free oocytes can be detected easily and extracted using a pipette from the loading chamber (Movie S5). Because the distance between the pillars is smaller than the oocyte diameter, no oocytes are lost after denudation. Finally, the cells are then transferred into another M2 media droplet for further analysis. Based on thermal images, there is negligible temperature fluctuations during VIF, and therefore, there should be no damage cells due to temperature fluctuations (Fotric 618C, Long Branch, NJ, USA).

Optimization of VIF oocyte denudation conditions

CR using VIF was investigated for two groups of mouse oocytes: fresh and freeze/thaw COCs. In VIF, CR is a function of HA concentration in the culture media, applied actuation power, and time exposure. Ideally, the lowest concentration of HA that can be used is preferred. Therefore, we chose 1.5 V_{pp} actuation power to identify the impact of different concentrations of HA on denudation time.

For both fresh and freeze/thaw oocytes, increasing the HA concentration allowed oocytes to be denuded faster (Fig. 6a). Freeze/thaw oocytes denuded more quickly at the same concentrations as fresh oocytes. We attribute this difference to the cumulus cells of fresh oocytes maintaining their integrity, and the higher concentration of hyaluronic acid in fresh COCs holds the cells tightly together. Conversely, the slow freezing and subsequent thawing of COCs damages

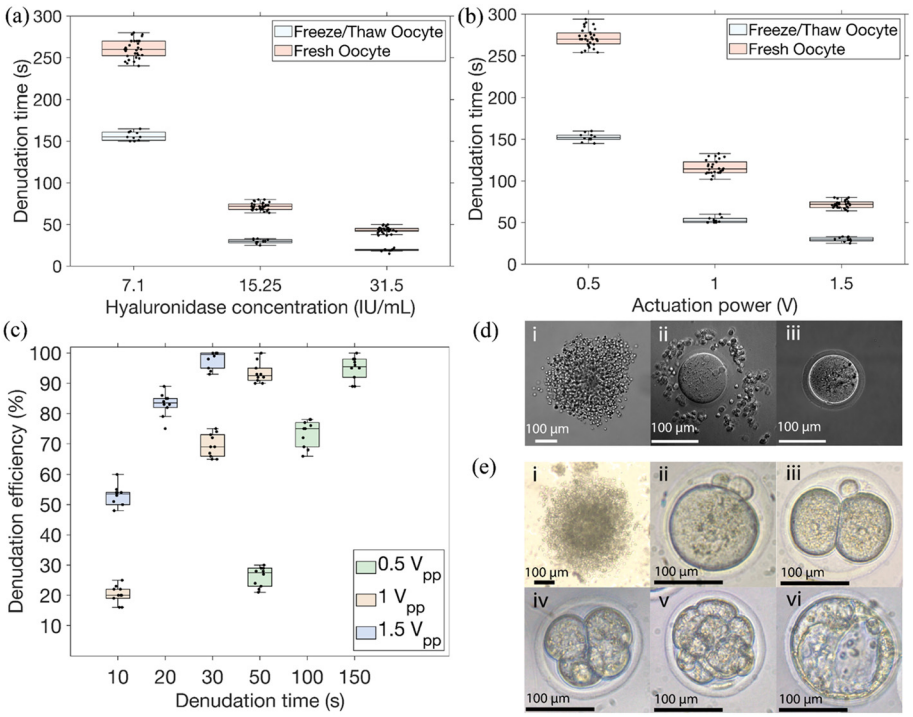

Fig. 6 Effect of different variables on oocyte cumulus removal, using vibration-induced flow (VIF). (a) The effect of hyaluronidase (HA) on oocyte denudation (P value < 0.05), while the applied actuation power is 1.5 V_{pp} for two groups of fresh and freeze/thaw oocytes. (b) The effect of applied actuation power on oocyte denudation (P value < 0.05) in 15.25 IU mL^{-1} HA solution for two groups of fresh and freeze/thaw oocytes. (c) Effect of actuation power and time exposure on denudation efficiency (P value < 0.05) of freeze/thaw oocytes, which shows a significant correlation between time exposure, applied actuation power, and denudation efficiency. (d) Representative images of (i) intact freeze/thaw oocyte, (ii) partially denuded, and (iii) fully denuded using VIF. (e) Representative images of (i) intact fresh oocyte, (ii–vi) embryo development stages after denudation by VIF, including (ii) fertilization (2PN), (iii) 2-cell (iv) 4-cell, (v) morula, and (vi) blastocyst. Note: images were taken from different embryos denuded by VIF.

some of the cumulus cells and results in a degraded extracellular matrix, which is easier to CR. The population means for the fresh *versus* freeze/thaw oocytes denuded at different HA concentrations were found to be significantly different using two-way ANOVA ($p < 0.0001$).

Even though the fastest times for oocyte cumulus denudation were found at a concentration of 31.5 IU mL^{-1}, the perivitelline space (PVS) expanded after the denudation. This expansion indicated mechanical stress and reduced oocyte integrity (Fig. S5). At lower HA concentrations, however, the PVS remained intact. Therefore, to ensure cell integrity after denudation, the effect of VIF on oocyte denudation using our platform was investigated at 15.25 IU mL^{-1} to continue our experiments.

We studied the effect of vibrational amplitude on CR for both groups (Fig. 6b). Using 15.25 IU mL^{-1} HA, the actuation power was adjusted from 0.5 to 1.5 V_{pp}. Decreasing the applied vibration amplitude to the system required additional time for the oocytes to denude because the induced velocity of the COCs moving in the chamber decreases. The slower velocity decreases the effect of shear force on the cell compared to a higher applied actuation power. Similar to the effect of HA concentration, the fresh samples denuded more slowly than the freeze–thaw samples. The time to denudation was significantly different between the two groups as indicated using two-way ANOVA ($p < 0.0001$).

Applied actuation power and exposure time directly affect CR, leading to varying denudation efficiencies. The device's denudation performance was studied at different actuation power levels and exposure times. Denudation efficiency is calculated as follows:

$$E_D = \frac{A_{untreated} - A_{treated}}{A_{untreated}} \quad (2)$$

where E_D is the denudation efficiency, and A represents the area of cumulus cells, determined through image processing techniques applied to the oocyte images taken before ($A_{untreated}$) and after ($A_{treated}$) the procedure by phase contrast microscope. To compare the actuation power for CR, we used 0.5 V_{pp}, 1 V_{pp}, and 1.5 V_{pp} to achieve different applied actuation amplitudes to the system over different exposure times. As expected, the denudation efficiency increased with higher driving applied actuation power and a longer exposure time (Fig. 6c). ANCOVA's analysis shows that the population means for applied amplitude power and exposure time differ significantly ($p < 0.0001$).

In addition to using our chip to denude individual oocytes, we evaluated the device's capacity to perform CR on a batch of cells. Efficient CR for freeze/thaw COCs was performed simultaneously for 15 oocytes in 30 s (Movie S6). We found the device capacity to be 20 to 23 cells for both fresh and freeze/thaw COC; beyond this number, some cells lacked sufficient contact with the pillars and were not completely denuded. From each superovulated female mouse, approximately 15–25 COCs can be collected. In manual CR, each COC must be denuded individually. In our system, we are able to denude all of the collected COCs in one batch, making the process more efficient overall for standard mouse IVF procedures. All the experiments were carried out in triplicate and confirmed the chip's ability to denude a batch of COCs. No oocytes were lost after the denudation. Images of intact freeze/thaw oocytes (Fig. 6d(i)) and cumulus denudation over time show partially denuded (Fig. 6d(ii)) and completely denuded (Fig. 6d(iii)) COCs achieved using our chip and VIF.

Fertilization and development potential of vibrational denuded oocytes

Fresh COCs were collected and inseminated. The inseminated COCs were denuded by manual pipetting *versus* VIF and then the fertilization rate was assessed by their ability to reach the two-pronuclei (2PN) stage of embryo development. Then the development potential of fertilized COCs was assessed by their ability to reach the blastocyst stage (Fig. 6e(i–vi)).

The control sample consisted of 54 inseminated oocytes denuded by manual pipetting. The VIF experiments were conducted on 58 inseminated oocytes denuded using 1 V_{pp} actuation power in human tubal fluid (HTF) medium without additional HA because, after insemination, the hyaluronic acid that holds the COC together has been degraded sufficiently. After denudation, we tracked all stages of preimplantation development under a microscope.

Successful fertilization was confirmed by the presence of two pronuclei at ~6–8 hours post-insemination. Embryos were evaluated for progression to the 2-cell stage at ~24 hours, morula at ~60–72 hours, and blastocyst at ~96–108 hours after IVF. After careful review of the embryo development stage, no notable difference in abnormal cleavage or embryo fragmentation were found between these groups.

Oocyte fertilization (2PN) rates from the two groups of denuded inseminated oocytes were not significantly different with 90.7% for manual pipetting and 93.1% for VIF (Fig. 6e(ii), P value = 0.65, by chi-square analysis). The blastulation rates were also not significantly different at 50.0% for manual pipetting, and 43.1% for VIF (Fig. 6e(vi), P value = 0.67, by chi-square analysis) (Table 1). There was no difference in all stages of early embryonic development

Table 1 Comparison of fertilization rate and early embryonic development by *in vitro* fertilization (IVF) of oocytes denuded by manual pipetting *versus* vibration-induced flow (VIF)

IVF cycle	Control (manual pipetting)	VIF (1 V_{pp})	P value
Number of cells	54	58	
Fertilization (2PN)	49 (90.7%)	54 (93.1%)	0.65
Two-cell	42 (77.8%)	40 (68.9%)	0.18
Four-cell	35 (64.8%)	35 (60.3%)	0.59
Morula	31 (57.4%)	30 (51.7%)	0.72
Blastocyst	27 (50.0%)	25 (43.1%)	0.67

between the two methods of oocyte denudation, indicating that VIF does not impact oocyte developmental potential.

Conclusion

We have developed a disposable chip for particle separation and oocyte denudation *via* VIF without using any oil or glass surface on top which makes oocyte retrieval a single-step process *via* pipette. The chip is easily mounted on the chip holder, enabling convenient access to cells and particle loading and collection. Using 13 μm particles, we demonstrated how actuation power and exposure time affect microparticle removal, achieving 99% cleaning efficiency. This is beneficial for lab-on-a-chip particle separation, maintaining clean detection areas, and enabling easy collection of larger particles. Then, using a mixture of smaller and larger particles (80 μm from 13 μm), we demonstrated that the larger particles remain inside the loading chamber, while the smaller particles are swept through the pillars to the annulus well when VIF is applied to the chip. The orientation of the pillars can be controlled, suggesting that this concept is applicable to particle separation, sorting, and collection.

Both fresh and freeze/thaw COCs can be treated with HA and VIF on-chip to achieve oocyte denudation. The smaller cumulus cells (~20 μm) were separated from the oocyte (~100 μm) by applying shear force to the COC as they bumped along the interior chamber pillars and were swept to the annulus well by the whirling flow through the pillars. The time to denudation of fresh oocytes was longer than for freeze/thaw oocytes, likely due to the preserved extracellular matrix of the fresh oocytes. The clean oocyte then remains in the loading chamber as its size precludes it from being swept away.

Higher applied amplitude and increased HA concentration slightly expanded the PVS, indicating possible mechanical stress; therefore, parameters were optimized to avoid any damage to the oocyte. We also found that we could affect CR for a batch of up to 23 COCs, enhancing the efficiency and reproducibility of the procedure.

Finally, using IVF, we conducted a biological assessment to ensure that there were no signs of mechanical damage to the oocytes after CR. During the embryo development for all groups of manual pipetting or VIF denuded oocytes, no instances of significant abnormal cleavage or embryo fragmentation were observed. This setup minimizes the potential contamination and allows for easy cell loading and collection in a thermally stable culture medium.

This VIF platform successfully reduces labor and time while maintaining the quality of the oocytes. The shear force used to achieve CR was handled electronically, and because the entire process can be done on an open-surface chip, no external pumps, lasers, or micromanipulators are needed. This system is portable, low-cost, and ideal for consistent, easier oocyte denudation. It also extends procedures to geographical areas lacking skilled embryologists or well-funded labs, reducing overall costs. Based on our preliminary studies, our VIF platform is a viable method for oocyte denudation that reduces time, increases reliability and can be used after insemination without impacting fertilization rates. We plan to extend our work to denudation prior to ICSI procedures as well as to isolate cancer cells from healthy cells.

Materials and methods

Open surface chip fabrication process

The fabrication process is shown in Fig. 1e. We fabricated the master mold on an acrylic sheet (McMaster Carr, 8505K754) using a CNC Milling Machine (X8-2200L, Beijing, CN). Polydimethylsiloxane (PDMS, Dow Sylgard 184 Silicone Encapsulant Clear 0.5 KG Kit, Ellsworth Adhesive, Germantown, WI) was prepared by mixing the prepolymer and its curing agent at a weight ratio of 10 : 1. The PDMS was poured over the mold and cured in a 65 °C oven for at least two hours. Finally, the PDMS was peeled from the mold (Fig. 1f and g). Three factors were considered in design and fabrication: micropillar height, micropillar diameter, and pattern of micropillars. The micropillar height was set to 1.1 mm because there is no glass cover or oil on top of the micropillar array; therefore, to achieve a stable rotation, the micropillar height must be higher than the height of the annulus well wall, which is 300 μm. Also, the pillar's height needs to fully cover the cell and should exceed the height of the cumulus–oocyte complex (400–700 μm). The pillar diameter is 300 μm.

Particle sample preparation

Microparticles used in the particle separation experiments are 13 μm red with an emission wavelength of 612 nm, an excitation wavelength of 542 nm, and purchased from Thermo Fisher Scientific (CAT. NO. 36-4, Waltham, MA, USA). The 80 μm green dry fluorescent polystyrene divinylbenzene microspheres have an emission wavelength of 508 nm, an excitation wavelength of 468 nm and were purchased from Thermo Fisher Scientific (CAT. NO. 35-10, Waltham MA, USA). Particle density is 1.05 g cm^{-3}. To stabilize the solution and avoid particle agglomeration, particles were suspended in the Milli-Q grade water (Millipore Inc., Bedford, MA, USA) containing 0.2% Tween 20 (Sigma-Aldrich, St. Louis, MO, USA CAS Number: 9005-64-5). The particle solution was vortexed to ensure that all small particles were distributed uniformly.

Particle image velocimetry (PIV) analysis

We used micro-particle image velocimetry (PIV) for flow visualization and to analyze the flow around the pillars (Fig. 3a) and track particle trajectories in the chip during VIF actuation. We obtained the velocity field by correlating particle movements from consecutive images using Mathworks Matlab R2024b software. The average flow velocity

field was calculated from 60 rotation cycles. The tracer particle *via* VIF on an observation plane was captured by superimposing consecutive images taken at 0.03-second intervals. To check the particle separation efficiency and to count the number of particles that move out of the loading chamber section, we excited the fluorescent particles by irradiating a sheet laser on the chip before and after the effect of VIF on the particle manipulation. We used ImageJ, v1.8.0 software, to count the number of particles inside the chamber.

Animals

C57BL/6J mice were bred in-house for all experiments in this study. Mice were housed in 11.5″ × 7.5″ IVC Polycarp Shoebox Cage for the duration of the experiment. Temperature 20–25 °C and humidity between 30 to 70% were maintained in the rodent room. Lights were turned ON from 5 AM and OFF at 7 PM in the rodent room.

Acquisition and preparation of gametes

For preliminary tests and optimization steps, we used sample mouse oocytes metaphase II (B6C3F1) with intact COCs commercially available and purchased from Embryotech Laboratories Inc. (Haverhill, MA, USA). The oocytes were cryopreserved using a slow-freeze method. The COCs were thawed prior to the experiments in an EmbryoMax M2 liquid medium (1X) with phenol red (Sigma-Aldrich, St. Louis, MO, USA. Product Number MR-015-D) following an established protocol.[51]

To obtain fresh COCs, 21–23-day-old C57BL6 female mice were injected intraperitoneally with 5 IU pregnant mare serum gonadotropin (PMSG, NATE-0969, Creative Enzymes) followed 44–48 hours later with the injection of 5 IU human chorionic gonadotropin (hCG, 9002-61-3, Sigma Aldrich). About 14–16 hours post hCG injection, the mice were euthanized by CO_2 inhalation followed by cervical dislocation. The oviducts were surgically removed and placed in human tubal fluid medium (HTF, MR-070-D, EMD Millipore Corporation). The ampullae were punctured by a 25-gauge needle to release the COC cluster. Once released, the COCs were carefully placed into clean HTF droplets by needle.

To obtain spermatozoa, the cauda epididymis of 4-month-old C57BL6 male mice was retrieved surgically and transported in HTF medium. The spermatozoa were released into a clean HTF medium droplet by microdissection. The spermatozoa were incubated at 37 °C, 5% CO_2 and for 1 hour prior to being used for IVF.

IVF procedure and embryo culture

For insemination, COCs were transferred into HTF medium under mineral oil, and 5–10 μL of capacitated sperm suspension was added (final sperm concentration ~1–2 × 10^5 mL^{-1}). After 3 hours of insemination at 37 °C in 5% CO_2, oocytes were allocated for manual washing or VIF denudation in HTF medium. Denuded oocytes were then transferred to KSOM drops (MR-106-D, EMD Millipore Corporation) under oil for continued *in vitro* culture at 37 °C in 5% CO_2.

Oocyte loading procedure

We used a 1 mm pipette tip during the transferring and washing steps to avoid manual denudation. We preloaded the chip with media EmbryoMax M2 liquid medium (1×) with phenol red and hyaluronidase (M2 + HA) (Sigma-Aldrich Product Number MR-051) (15.25 IU mL^{-1}) prior to loading the cells into the chamber. The samples were loaded into the chip and allowed to degrade the cumulus cells matrix surrounding the oocytes with the HA for 1 min without agitation, and before VIF was applied. After denudation, cells were transferred to a drop of M2 medium on a Petri dish for washing and evaluation of denudation efficiency, and phase-contrast microscopy was used to capture images.

Statistical analysis

Statistical analysis was performed using JMP Pro (Version 17, SAS Institute, USA) with a significance level set at $p < 0.05$ to determine any significant differences. A two-way ANOVA was used to evaluate the effect of actuation power and HA on CR for both groups of fresh and freeze–thawed oocytes. ANCOVA analysis was used to evaluate the denudation efficiency. A chi-square test was used to compare the developmental stages between the control and VIF-treated CR.

Ethical statement

All animal procedures were performed in accordance with the Guidelines for Care and Use of Laboratory Animals of Cornell University and approved by the Institutional Animal Care and Use Committee (IACUC) of Cornell University per approved protocol number 2019-0006.

Author contributions

A. F. was responsible for conceptualization, methodology, formal analysis, data curation, investigation, device design, device fabrication, software, writing – original draft, and review & editing; A. M. was responsible for conceptualization, methodology, data curation, investigation, device design, device fabrication, and software. H. Z. was responsible for data curation, investigation, writing – review & editing. Y. A. R. was responsible writing – review & editing, and supervision. A. A. was responsible for project administration, funding acquisition, writing – review & editing, and supervision.

Conflicts of interest

The authors declare no conflicts of interest.

Data availability

Supplementary information: The supplementary data includes additional figures, tables and discussion. See DOI: **https://doi.org/10.1039/D5LC00414D**.

All raw data used to generate the figures in this manuscript are available at: **https://doi.org/10.5281/zenodo.15133111**.

Acknowledgements

The authors would like to thank Dr. Soon Hon Cheong for his thoughtful comments during the experiments. This work was performed in part at the Cornell NanoScale Science & Technology Facility (CNF), a member of the National Nanotechnology Coordinated Infrastructure NNCI, which is supported by the National Science Foundation (Grant NNCI-2025233). The authors also thank Dr. Kelley J. Donaghy for editing and proofreading.

The authors certify that generative AI was not used in preparing this article. Non-generative AI, such as spelling and grammar checkers in Office 365 and Google Docs, and citation managing software, was used. All instances when non-generative AI was used were reviewed by the authors and editors.

References

1 GBD 2021 Fertility and Forecasting Collaborators, *Lancet*, 2024, **403**, 2057–2099.
2 M. Jain and M. Singh, *Assisted reproductive technology (ART) techniques*, 2022.
3 T. Ebner, in *In Vitro Fertilization*, ed. Z. P. Nagy, A. C. Varghese and A. Agarwal, Springer International Publishing, Cham, 2019, pp. 471–479.
4 G. Palermo, H. Joris, P. Devroey and A. C. Van Steirteghem, *Lancet*, 1992, **340**, 17–18.
5 A. R. Thornhill, C. E. deDie-Smulders, J. P. Geraedts, J. C. Harper, G. L. Harton, S. A. Lavery, C. Moutou, M. D. Robinson, A. G. Schmutzler and P. N. Scriven, *Hum. Reprod.*, 2005, **20**, 35–48.
6 M. F. Meyer, G. Kreil and H. Aschauer, *FEBS Lett.*, 1997, **413**, 385–388.
7 H. Van de Velde, Z. P. Nagy, H. Joris, A. De Vos and A. C. Van Steirteghem, *Hum. Reprod.*, 1997, **12**, 2246–2250.
8 H. C. Zeringue and D. J. Beebe, in *Germ Cell Protocols*, Humana Press, New Jersey, 2004, vol. 254, pp. 365–374.
9 H. C. Zeringue, J. J. Rutledge and D. J. Beebe, *Lab Chip*, 2005, **5**, 86–90.
10 L. Weng, G. Y. Lee, J. Liu, R. Kapur, T. L. Toth and M. Toner, *Lab Chip*, 2018, **18**, 3892–3902.
11 M. Yaghoobi, A. Abdelhady, A. Favakeh, P. Xie, S. Cheung, A. Mokhtare, Y. L. Lee, A. V. Nguyen, G. Palermo and Z. Rosenwaks, *Lab Chip*, 2024, **24**, 210–223.
12 A. Karimi, M. Yaghoobi and A. Abbaspourrad, *Lab Chip*, 2025, **25**, 631–643.
13 M. Zaferani, S. H. Cheong and A. Abbaspourrad, *Proc. Natl. Acad. Sci. U. S. A.*, 2018, **115**, 8272–8277.
14 R. Ma, L. Xie, C. Han, K. Su, T. Qiu, L. Wang, G. Huang, W. Xing, J. Qiao, J. Wang and J. Cheng, *Anal. Chem.*, 2011, **83**, 2964–2970.
15 R. S. Suh, X. Zhu, N. Phadke, D. A. Ohl, S. Takayama and G. D. Smith, *Hum. Reprod.*, 2006, **21**, 477–483.
16 D. Lai, J. Ding, G. W. Smith, G. D. Smith and S. Takayama, *Hum. Reprod.*, 2015, **30**, 37–45.
17 H. Kutluk, M. Viefhues and I. Constantinou, *Small Sci.*, 2024, **4**, 2300206.
18 R. Franko and M. de A. M. M. Ferraz, *Lab Chip*, 2025, **25**, 187–200.
19 T. Hayakawa, S. Sakuma, T. Fukuhara, Y. Yokoyama and F. Arai, *Micromachines*, 2014, **5**, 681–696.
20 A. Y. Fu, H.-P. Chou, C. Spence, F. H. Arnold and S. R. Quake, *Anal. Chem.*, 2002, **74**, 2451–2457.
21 G. Carmon and M. Feingold, *Opt. Lett.*, 2010, **36**, 40–42.
22 A. Ramadan, K. Inoue, T. Arai and T. Takubo, *Adv. Robot.*, 2008, **22**, 235–260.
23 A. Ozcelik, N. Nama, P.-H. Huang, M. Kaynak, M. R. Mcreynolds, W. Hanna-Rose and T. J. Huang, *Small*, 2016, **12**, 5120–5125.
24 A. Favakeh, A. Mokhtare, M. J. Asadi, J. C. M. Hwang and A. Abbaspourrad, *Lab Chip*, 2025, **25**, 1744–1754.
25 A. Favakeh, M. A. Bijarchi, M. Mohammadrashidi, M. Yaghoobi and M. B. Shafii, *PLoS One*, 2025, **20**, e0321099.
26 A. Ashkin, J. M. Dziedzic and T. Yamane, *Nature*, 1987, **330**, 769–771.
27 L. Y. Yeo and J. R. Friend, *Biomicrofluidics*, 2009, **3**(1), 012002.
28 J. Voldman, M. L. Gray, M. Toner and M. A. Schmidt, *Anal. Chem.*, 2002, **74**, 3984–3990.
29 F. A. García-Vázquez, G. Garrappa, C. Luongo, J. G. Hamze, M. Caballero, F. Marco-Jiménez, J. S. Vicente Antón, G. J. Molina-Cuberos and M. Jiménez-Movilla, *Adv. Sci.*, 2024, **11**, 2306901.
30 T. Hayakawa, S. Sakuma and F. Arai, *Microsyst. Nanoeng.*, 2015, **1**, 1–9.
31 T. Sato, K. Kaneko, T. Hayakawa and H. Suzuki, *Micromachines*, 2023, **14**, 2010.
32 T. Hayakawa, Y. Akita and F. Arai, *Microfluid. Nanofluid.*, 2018, **22**, 42.
33 Y. Zhou, Z. Ma and Y. Ai, *Anal. Chem.*, 2020, **92**, 12795–12800.
34 Y. Zhou, H. Wang, Z. Ma, J. K. W. Yang and Y. Ai, *Adv. Mater. Technol.*, 2020, **5**, 2000323.
35 T. Hayakawa, Y. Akita and F. Arai, in *2017 IEEE 30th International Conference on Micro Electro Mechanical Systems (MEMS)*, IEEE, 2017, pp. 1281–1284.
36 H. Kobayashi, Y. Koike and T. Hayakawa, in *2023 IEEE/SICE International Symposium on System Integration (SII)*, IEEE, 2023, pp. 1–4.
37 V. H. Lieu, T. A. House and D. T. Schwartz, *Anal. Chem.*, 2012, **84**, 1963–1968.
38 B. R. Lutz, J. Chen and D. T. Schwartz, *Anal. Chem.*, 2006, **78**, 5429–5435.
39 K. Nakahara, S. Sakuma, T. Hayakawa and F. Arai, in *2015 International Symposium on Micro-NanoMechatronics and Human Science (MHS)*, IEEE, 2015, pp. 1–3.
40 A. Mokhtare, B. Davaji, P. Xie, M. Yaghoobi, Z. Rosenwaks, A. Lal, G. Palermo and A. Abbaspourrad, *Lab Chip*, 2022, **22**, 777–792.
41 A. Mokhtare, P. Xie, A. Abbaspourrad, Z. Rosenwaks and G. D. Palermo, *Fertil. Steril.*, 2020, **114**, e76.

42 R. Zhai, G. Shan, C. Dai, M. Hao, J. Zhu, C. Ru and Y. Sun, *Micromachines*, 2022, **13**(8), 1301.
43 A. Mokhtare, A. Favakeh, P. Xie, Z. Rosenwaks, A. Abbaspourrad and G. Palermo, *FS Sci.*, 2025, **6**, 118–125.
44 L. Rayleigh, *Philos. Trans. R. Soc. London*, 1884, **175**, 1–21.
45 C. Y. Wang and B. Drachman, *Appl. Sci. Res.*, 1982, **39**, 55–68.
46 T. Hayakawa, S. Sakuma and F. Arai, in *2015 IEEE/RSJ International Conference on Intelligent Robots and Systems (IROS)*, IEEE, 2015, pp. 1409–1414.
47 S. Awtar and G. Parmar, *J. Mech. Robot.*, 2013, **5**, 021008.
48 J. Zhou, D. A. Khodakov, A. V. Ellis and N. H. Voelcker, *Electrophoresis*, 2012, **33**, 89–104.
49 C. Han, Q. Zhang, R. Ma, L. Xie, T. Qiu, L. Wang, K. Mitchelson, J. Wang, G. Huang, J. Qiao and J. Cheng, *Lab Chip*, 2010, **10**, 2848–2854.
50 N. Tsampras, M. Kollmann and L. Craciunas, *J. Obstet. Gynaecol.*, 2022, **42**, 301–305.
51 H. Hedrich, *The Laboratory Mouse*, Academic Press, 2004.

